processes

MDPI

Article

Study of the Factors Limiting the Efficiency of Vertical-Type Nitride- and AlInGaP-Based Quantum-Well Micro-LEDs

Cheng-Han Ho †, Shih-Min Chen † and Yuh-Renn Wu *,†

Graduate Institute of Photonics and Optoelectronics and Department of Electrical Engineering, National Taiwan University, Taipei 10617, Taiwan; r08941065@ntu.edu.tw (C.-H.H.); r10941030@ntu.edu.tw (S.-M.C.)

* Correspondence: yrwu@ntu.edu.tw

† These authors contributed equally to this work.

Abstract: The efficiency of micro-light-emitting diodes (μ-LEDs) depends enormously on the chip size, and this is connected to sidewall-trap-assisted nonradiative recombination. It is known that the internal quantum efficiency (IQE) of aluminum gallium indium phosphide (AlGaInP)-based red μ-LEDs is much lower than that of nitride-based μ-LEDs. To establish the major reasons giving rise to this huge IQE discrepancy, we examined the limiting factors in the two structures. For the nitride-based InGaN quantum wells, the influences of random alloy fluctuations were examined. A two-dimensional Poisson and drift-diffusion solver was applied to analyze these issues.

Keywords: AlGaInP-based red μ-LEDs; sidewall-trap; nitride-based μ-LEDs; random alloy fluctuations

Citation: Ho, C.-H.; Chen, S.-M.; Wu, Y.-R. Study of the Factors Limiting the Efficiency of Vertical-Type Nitride- and AlInGaP-Based Quantum-Well Micro-LEDs. *Processes* **2022**, *10*, 489. https://doi.org/10.3390/pr10030489

Academic Editor: Wei-Chih Lai

Received: 10 February 2022
Accepted: 27 February 2022
Published: 28 February 2022

Publisher's Note: MDPI stays neutral with regard to jurisdictional claims in published maps and institutional affiliations.

Copyright: © 2022 by the authors. Licensee MDPI, Basel, Switzerland. This article is an open access article distributed under the terms and conditions of the Creative Commons Attribution (CC BY) license (https://creativecommons.org/licenses/by/4.0/).

1. Introduction

In the pursuit of higher-resolution miniature displays in applications such as augmented or virtual reality [1] and displays with transparent areas [2], the size of light-emitting diodes (LEDs) has been decreasing. Nevertheless, many studies have found that the efficiency of micro-LEDs (μ-LEDs) decreases with chip size because of sidewall trapping effects [3–5]. Different passivation methods have been proposed to reduce sidewall trapping effects and improve efficiency [6,7]. For instance, plasma-enhanced chemical vapor deposition and atomic layer deposition [8] have been proposed to deposit oxides for surface passivation [9]. In addition to experimental approaches to improving efficiency, it is important to establish the key factors leading to carrier diffusion into the sidewall.

It is known that red LEDs based on aluminum gallium indium phosphide (AlGaInP) suffer from severe sidewall trapping effects as the chip size shrinks [10–13]. This might be due to the lower effective mass and larger carrier mobility in AlGaInP-based quantum wells (QWs). However, the efficiency decrease in nitride-based (e.g., indium gallium nitride (InGaN)) LEDs is much smaller [14–19]. It has been found that random alloy fluctuations will limit carrier diffusion in an InGaN quantum system [20]; the inhomogeneous bandgap distribution resulting from these fluctuations enhances carrier localization and limits carrier diffusion [21,22]. In addition, although the AlGaInP is also an alloy material, it has a smaller potential fluctuation due to the smaller bandgap difference as the composition changes. The effective mass is smaller and contributes to weaker confinement. In contrast, the polarization field increases the diffusion length as a result of decreases in radiative recombination rates [20].

In addition to these effects in QWs, the electron and hole transport layers, the electron blocking layers, and quantum barriers (QBs) may play roles in these problems. To investigate the influences of each of these factors, it is important to have a proper simulation tool. Our past research employed a three-dimensional (3D) simulation tool to study the phenomenon of alloy fluctuations at the nanoscale, and we demonstrated the influence of alloy disorder without using any approximations [23]. However, because of memory-usage

limitations in these 3D simulations, it is challenging to operate them at µm scales, which includes atomic-scale random alloy fluctuations. Hence, a two-dimensional (2D) simulation that contains random alloy fluctuations is an alternative way to study these phenomena. In this work, we used a 2D simulator [24] to approximate the random alloy fluctuations and model the behavior of μ-LEDs. The structures of the LEDs that were examined in these simulations are shown in Figure 1. In addition to a 10-µm μ-LED, a 5-µm μ-LED (with one 2-µm n-pad and one 5-µm p-pad) and a 20-µm μ-LED (with four 2-µm n-pads and one 20-µm p-pad) were also simulated.

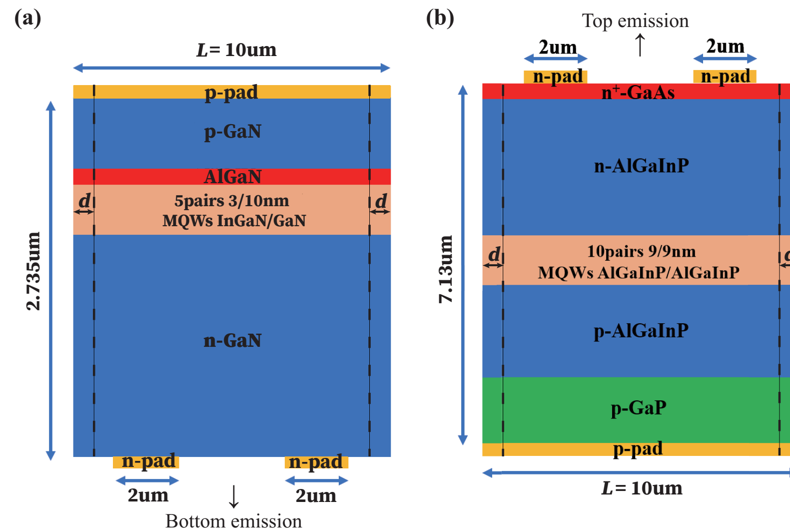

Figure 1. Structures of the 10-µm (**a**) blue and (**b**) red [11] LEDs, showing two 2-µm n-pads and one 10-µm p-pad. The depletion region (denoted by "d") near the QW is approximately 100 nm thick.

2. Methodology

A flowchart of the simulations is presented in Figure 2a. In this process, first, an in-house-developed fully-2D drift-diffusion charge-control solver (2D-DDCC) is used to analyze the electrical properties, carrier distribution, and other parameters of the devices [25–27]. Second, a random number generator is used to generate random atom distributions, and the Gaussian averaging method is adopted for the local indium composition in the QW [28]. The algorithm details are given in Refs. [23,29]. The local material parameters are then dependent on the local indium composition; specifically, these simulations examined the bandgap and polarization dipole. The potential can be then obtained by inserting these parameters into the Poisson equation,

$$\nabla \cdot (\varepsilon \nabla \psi) = q(n - p + N_A^- - N_D^+ \pm \rho_{\text{pol}}), \tag{1}$$

where: ψ is the potential of the structure; n and p are the free electrons and holes in the device, respectively; N_A^- and N_D^+ are the fixed charges based on the activation energy; and ρ_{pol} is the polarization that has been resolved. We replace the Schrödinger equation solver with the localization landscape,

$$\left(-\frac{\hbar^2}{2m_{e,h}^*}\Delta + E_{c,v}\right)u_{e,h} = 1, \tag{2}$$

in which $1/u_{e,h}$ is the effective quantum potential. This is similar to the actual potential, meaning that the problem can be solved more efficiently. Finally, the carrier distributions are computed using

$$n = \int_{1/u_e}^{+\infty} N_c(E) \cdot f_n(E) dE, \tag{3}$$

$$p = \int_{1/u_h}^{-\infty} N_v(E) \cdot f_p(E)dE, \quad (4)$$

and the effective potential and the carrier Fermi level are obtained using

$$J_{n,p} = \mu_{n,p}(n,p)\nabla E_{f_{n,p}}, \quad (5)$$

$$\frac{1}{q}\nabla(J_{n,p}) = R_{n,p} - G_{n,p}, \quad (6)$$

respectively. These equations are solved iteratively until the error is below a predefined threshold.

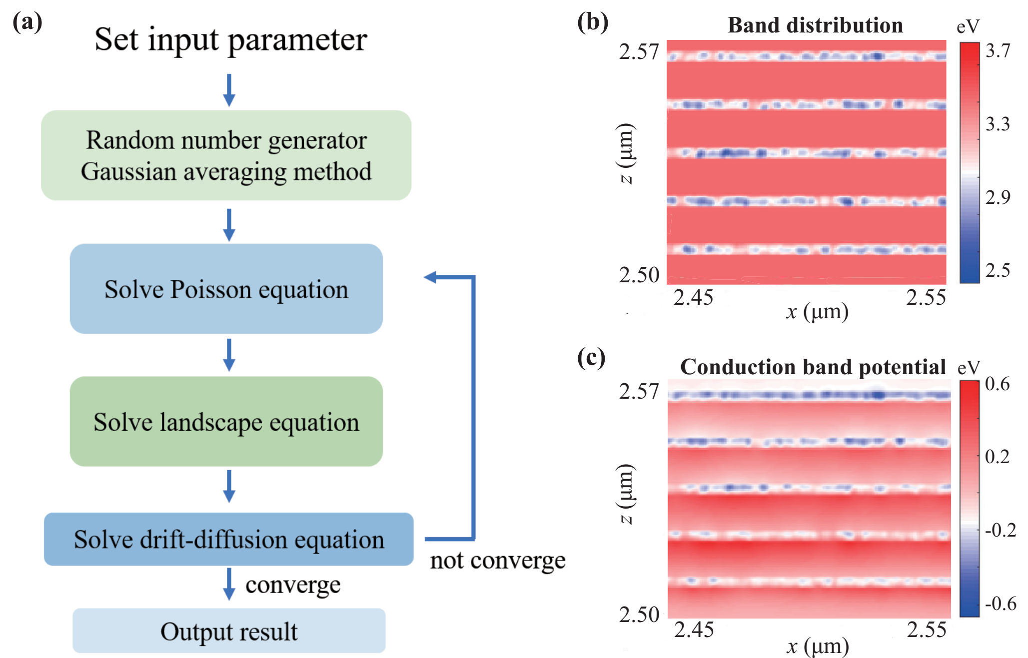

Figure 2. (**a**) Flow chart of the simulation model. (**b**) Bandgap distribution and (**c**) conduction band potential of the whole μ-LED with the random alloy fluctuations, which can be observed in the InGaN LED QWs. The fluctuating potential is a result of the inhomogeneous distribution of the bandgap.

The following equations are used in the 2D simulations:

$$R = \text{SRH} + B_0 np + C_0(n^2 p + np^2), \quad (7)$$

$$\text{SRH} = \frac{np - n_i^2}{\tau_{n0}(p + p_i) + \tau_{p0}(n + n_i)}, \quad (8)$$

where B_0 and C_0 are the radiative and Auger recombination coefficients, respectively. The recombination rate in Equation (7) comprises radiative recombination, Auger recombination and Shockley–Read–Hall (SRH) recombination [Equation (8)].

To discuss the sidewall effect, simulations of different chip sizes in the InGaN system for blue μ-LEDs and the AlGaInP system for red μ-LEDs are needed. For this part, we implemented composition fluctuations in the 2D simulations, but the alloy fluctuations were only applied to the blue μ-LEDs, since the potential variation in blue μ-LEDs is more significant.

3. Results and Discussion

This section can be divided into two parts. The first includes the electrical and optical properties of blue and red μ-LEDs with different chip sizes and the influence of the carrier mobility on blue μ-LEDs with random alloy fluctuations. The second considers the factors

that bring about the differences in internal quantum efficiency (IQE) between these two kinds of μ-LED.

3.1. Shrinking the Red and Blue μ-LEDs and the Mobility Distribution of the Blue μ-LEDs

As noted, when the chip size is reduced, the efficiency decreases because of the influences of sidewall trapping. In the 2D simulations, the sidewall areas were the same for each of the different chip sizes; however, the ratio of the sidewall to the total area increases as the chip size decreases. These sidewall traps behave as caves, and the carriers flow inside these traps and recombine nonradiatively through defects. As shown in Figure 3, the InGaN-based blue LEDs are influenced less by the chip size. However, the IQE drops significantly for the AlInGaP-based red LEDs, and the efficiency is less than 10% for the 5-µm chip size. This may be due to the larger diffusion length of AlInGaP-based QWs resulting from their higher carrier mobility and lower effective mass. In InGaN μ-LEDs, the lateral diffusion ability in the QW is strongly related to potential fluctuations resulting from the disordered composition [29], as depicted in Figure 2b,c. The parameters of the blue and red μ-LED are listed in Tables 1 and 2, respectively.

Table 1. Parameters of blue μ-LEDs.

Epi-Layer	p-GaN	p-AlGaN	p-GaN Cladding Layer	GaN QB/InGaN QW	n-GaN Cladding Layer	n-GaN
Thickness (nm)	140	20	10	10/3	10	2500
Bandgap (eV)	3.437	3.7194	3.437	3.437/2.8724	3.437	3.437
Doping (10^{18} cm^{-3})	30	20	2	0.01/0.01	5	5
Activation energy (meV)	180	264	180	25/25	25	25
B_0 coefficient (10^{-11} cm^3/s)	2	2	2	2/2	2	2
C_0 coefficient (10^{-30} cm^6/s)	0.1	0.1	0.1	0.1	0.1	0.1
τ_n (ns)	100	100	100	100	100	100
τ_p (ns)	100	100	100	100	100	100
τ_n at sidewall (ns)	0.1	0.1	0.1	0.1	0.1	0.1
τ_p at sidewall (ns)	0.1	0.1	0.1	0.1	0.1	0.1

Table 2. Parameters of red μ-LEDs.

Epi-Layer	p-GaP	p-AlGaInP	i-AlGaInP QB/QW	n-AlGaInP	n-GaAs
Thickness (nm)	2500	600	9/9	3500	100
Bandgap (eV)	2.26	2.21	2.21/1.97	2.21	1.42
Doping (10^{18} cm^{-3})	1	1	...	1	1
Activation energy (meV)	20	12.3	...	12.3	10
B_0 coefficient (10^{-11} cm^3/s)	0.01	8.25	(8.25/6.50)	8.25	70
C_0 coefficient (10^{-30} cm^6/s)	1	1	1	1	1
τ_n (ns)	100	100	100	100	100
τ_p (ns)	100	100	100	100	100
τ_n at sidewall (ns)	0.1	0.1	0.1	0.1	0.1
τ_p at sidewall (ns)	0.1	0.1	0.1	0.1	0.1

For a retangular chip size, the chip length and width is defined as L_x and L_y, respectively. The QW height is defined by H_z. The sidewall region size suggested in Ref. [30] is 120 nm. From Figure 1, the surface volume ratio—which is defined as the ratio of the sidewall volume to the total volume—is $2dL_yL_z : L_xL_yH_z = 2d : L_x$ in the 2D simulations, and in the 3D simulations, it is $4d'L_yH_z : L_xL_yH_z = 4d' : L_x$. Therefore, we set $d = 2d' = 240$ nm at both sides in our 2D simulation model to obtain the same surface volume ratio. The lifetime at the sidewall was set as 0.1 ns (Table 2). The graphs in Figure 3a,c present the IQE values for blue and red μ-LEDs, respectively. It can be seen that the IQE of the μ-LEDs declined prominently as the size decreased [12]. For the 5-µm red

LED, the efficiency was almost 0% at low current density. For the 5-µm blue LED, the IQE was maintained at about 50% at 20 A/cm^2. As noted above, one of the key elements that causes this difference might be the differing mobility of carriers in the QWs, which makes them diffuse to the sidewall faster or slower [31].

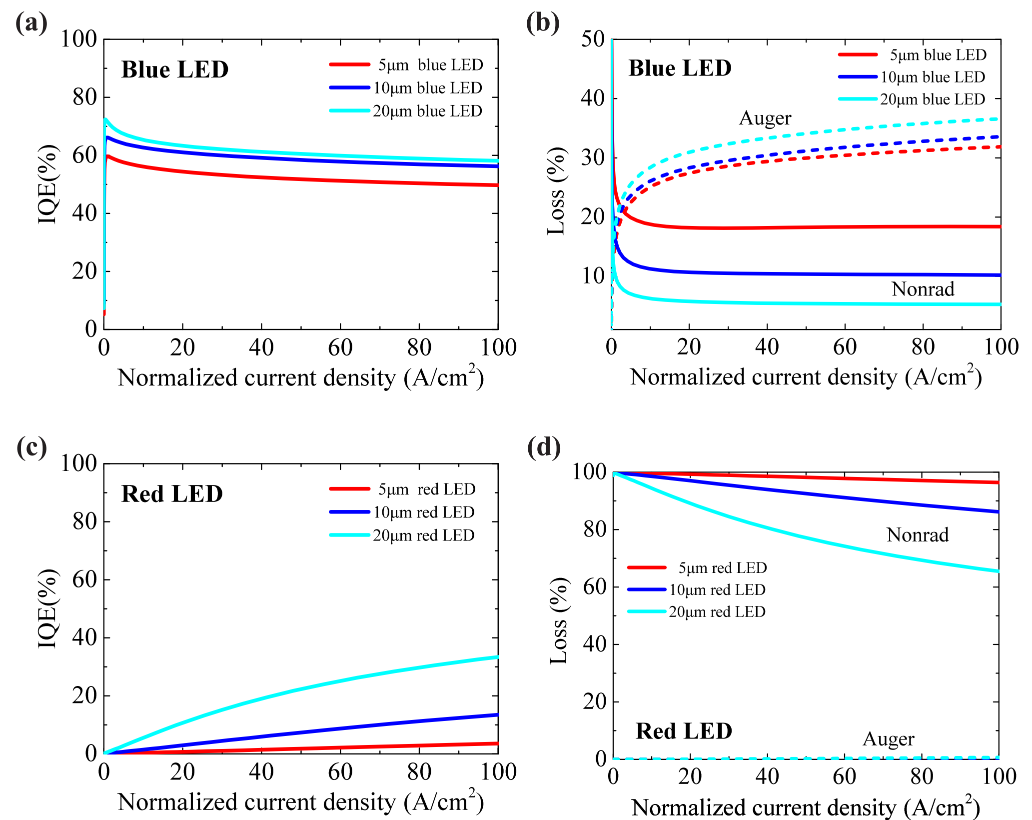

Figure 3. IQE of (**a**) blue and (**b**) red μ-LEDs with three different chip sizes that may be affected by SRH and Auger recombination, (**c**) for blue and (**d**) for red μ-LEDs.

The losses in the red μ-LEDs shown in Figure 3d are dominated by SRH nonradiative recombination at the sidewall regions [Figure 4d], and the Auger recombination is nearly 0% since the carriers are not crowded but instantly flow into the sidewall and recombine nonradiatively. Nonetheless, Figure 3b shows that the Auger recombination is greater than the SRH recombination in blue μ-LEDs; because the carriers are localized, their transport ability is limited. Thus, the currents will not easily flow to the sides. Although the nonradiative recombination rate at the sidewalls is large, it does not dominate. Figure 4a,b show that some of the carriers recombine at the sidewall, but there is still a large fraction that recombine in the central area.

Theoretically, the different mobility and the presence of indium composition fluctuations make the performance of blue μ-LEDs different from that of red μ-LEDs. In an attempt to examine this, supposing the carrier mobility in an InGaN QW is as high as that in an AlGaInP QW, from Figure 5, we notice that the IQE in the InGaN QW is still superior to that in the red LED, which indicates the influence of hidden factors that have not yet been revealed. Hence, we need to further examine these unknown factors influencing the IQE of μ-LEDs.

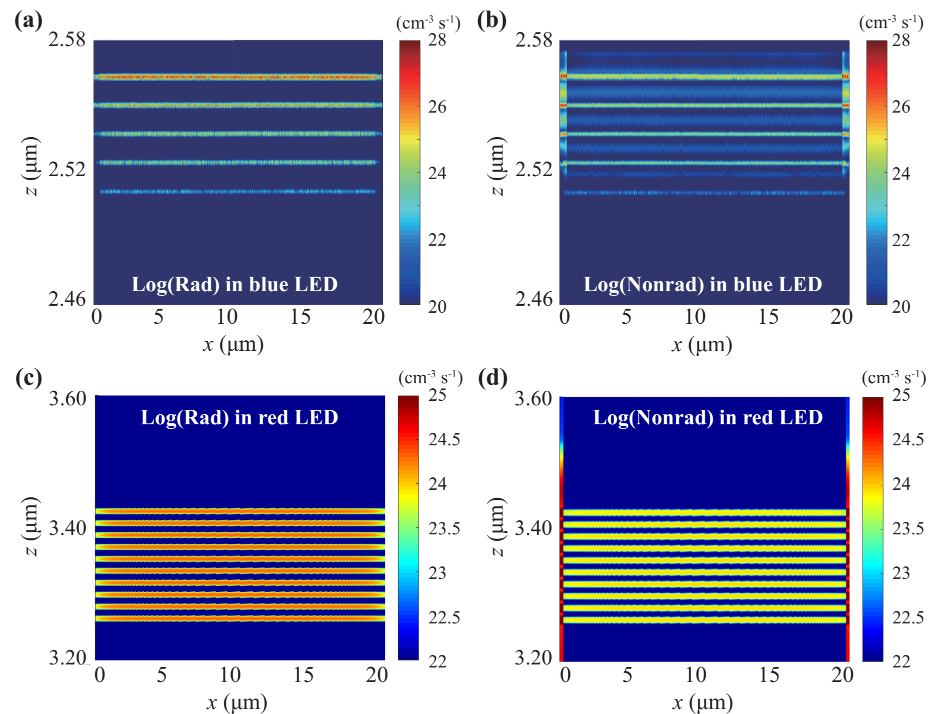

Figure 4. (**a**,**c**) Radiative and (**b**,**d**) non-radiative recombination rate (per unit volume per unit time) distributions at a current density of 20 A/cm^2 for the 20-µm blue and red LEDs with piezoelectric effect and random alloy fluctuations.

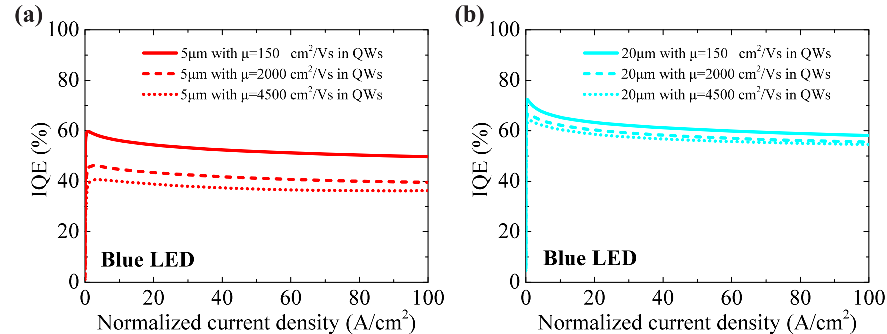

Figure 5. Influences of carrier mobility on the IQE of blue LED QWs with random alloy fluctuations: (**a**) 5 µm and (**b**) 20 µm dimensions. The carrier mobility in the blue LEDs (μ_n = 150 cm^2/Vs, μ_p = 10 cm^2/Vs) increases gradually to become identical to the mobility in the red LEDs ($\mu_n = 4500$ cm^2/Vs, $\mu_p = 190$ cm^2/Vs).

3.2. Influences of Random Alloy Potential Fluctuations, Piezoelectric Field, and p–n Layer Mobility

Since the higher carrier mobility in AlInGaP QWs is not the only reason for the lower IQE of red LEDs, we need to examine other parameters that influence the IQE of μ-LEDs. Aside from the difference in the bandgap, the parameter differences of blue and red include: (1) the piezoelectric polarization-induced quantum-confined Stark effect [32]; (2) the effects of random alloy fluctuations; (3) the mobility difference in the QW; (4) the effective mass difference in the QW; (5) the mobility difference in the QB; (6) the mobility difference between the n and p layers. These six factors are listed as different cases for parameter examination in Table 3.

Case 1 is a 20-µm blue LED without the piezoelectric effect, and the other 5 cases are adjusted on the basis of the preceding case by altering a specific factor (i.e., Case 2 differs from Case 1 by removing the fluctuations; Case 3 differs from Case 2 by strengthening the electron mobility ($\mu_n = 4500$ cm^2/Vs in QWs). In Figure 6a, we start by removing the

piezoelectric polarization (Case 1, the gray line) and random alloy fluctuations (Case 2, the red line) in the simulations of nitride-based LEDs, since the AlGaInP system does not have these effects. Under the condition that the random alloy fluctuations and piezoelectric effects are neglected, the IQE drops at low current density, which indicates that the carriers are not localized. Furthermore, the IQE peak shifts toward a much larger current density, and the droop effect disappears. This is due to better electron and hole overlap and a shorter radiative lifetime; the Auger effect will appear later because the carrier density will not be high enough due to the shorter lifetime.

Table 3. Comparison of the parameters in cases 1–6.

Parameter/Case Number	Case 1	Case 2	Case 3	Case 4	Case 5	Case 6
Piezoelectric effect	Yes ⇒ No	No	No	No	No	No
Fluctuation	Yes	Yes ⇒ No	No	No	No	No
e^- mobility in QWs (cm^2/Vs)	150	150	150 ⇒ 4500	4500	4500	4500
h^+ mobility in QWs (cm^2/Vs)	10	10	10 ⇒ 190	190	190	190
e^- effective mass in QWs (m_0)	0.157	0.157	0.157	0.157 ⇒ 0.0832	0.0832	0.0832
hh effective mass in QWs (m_0)	1.82	1.82	1.82	1.82 ⇒ 0.576	0.576	0.576
lh effective mass in QWs (m_0)	0.1338	0.1338	0.1338	0.1338 ⇒ 0.131	0.131	0.131
e^- mobility in QBs (cm^2/Vs)	350	350	350	350	350 ⇒ 4000	4000
h^+ mobility in QBs (cm^2/Vs)	10	10	10	10	10 ⇒ 180	180
e^- mobility in n layer (cm^2/Vs)	350	350	350	350	350	350 ⇒ 4000
h^+ mobility in p layer (cm^2/Vs)	10	10	10	10	10	10 ⇒ 180

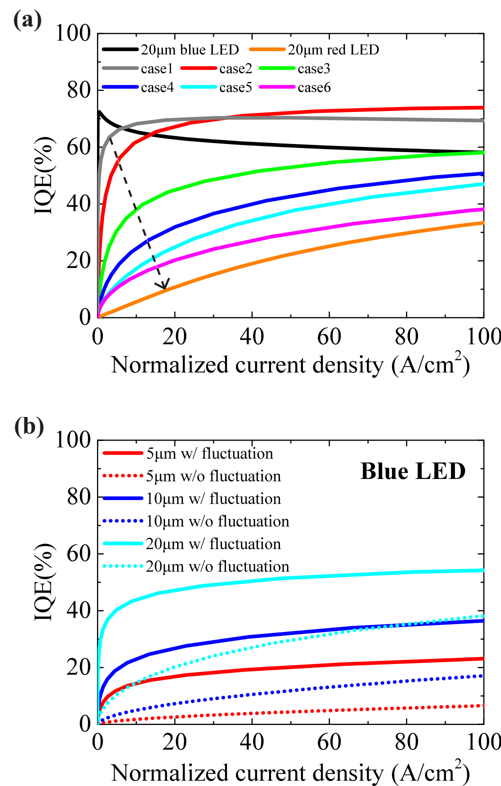

Figure 6. (**a**) Influence of different parameters on the IQE values of blue and red LEDs. The orange and black lines respectively indicate the 20-µm blue and 20-µm red LEDs presented as 2 cyan lines in Figure 3a,c. (**b**) IQE of blue LEDs in Case 6 for 3 types of sizes with and without random alloy fluctuations.

From Case 3 to Case 6, we can find that the QW, QB, and p and n layers all play roles in spreading the current and influencing the IQE. In cases 3 and 4, the mobility and

effective mass of the nitride material are changed to be as high as those in AlInGaP, where a significant drop of IQE is observed. This can be explained to be the result of the large diffusion coefficient due to the higher mobility and effective mass. However, changing these two factors still leads to a higher IQE than that found in the AlInGaP-based red LEDs. After we further set the mobility of the QB and the p and n layers to be the same as in the AlInGaP-based red LEDs, the result gradually approaches the performance of AlInGaP.

In summary, there is more than just one cause keeping the IQE low in red μ-LEDs. The effective mass and even the mobility in the QB (which might affect the current spreading) will diminish the IQE; the current may already diffuse to the sidewall before reaching the QW. However, for nitride material, the p-GaN layer has a lower mobility, which turns out to be a positive factor that can maintain relatively higher efficiency in μ-LED applications.

These results indicate that to improve efficiency in red LEDs, weakening the carrier mobility in all layers (QW/QB) is needed to improve the IQE in μ-LED applications. Moreover, as noted previously, random alloy fluctuations contribute to localizing the carriers and restricting transport such that most carriers will diffuse vertically (few carriers flow into the sidewall region), providing a better IQE. As Figure 6b shows, we consider fluctuations in Case 6 (dashed line) for another case (solid line); the outcome shows that the fluctuations increase the IQE in this simulation work. In other words, the IQE for red LEDs [Figure 3c] may be increased by imposing fluctuations on its QWs. The results also suggest that increasing the resistivity in the p and n layers might be good for μ-LED applications; this is in contrast to standard-sized LEDs, in which a lower resistivity is always preferable. In addition, for AlInGaP based red LEDs, it is hard to confine carriers with alloy potential fluctuation due to smaller effective mass and the smaller band offset energy difference. Hence, using the QD-like structure would help to build up deeper potential to confine carriers and limit the lateral diffusion of carriers. This will provide similar effect to the random alloy fluctuation in the InGaN QW system.

4. Conclusions

The influences of the mobility and random alloy potential fluctuations in the nitride system were analyzed and compared with the AlGaInP red LED system. The results suggest that, aside from potential fluctuations or mobility differences in the QWs, there are additional factors that can each play a role in limiting the efficiency. The mobility in the QB or the n and p layers and the effective mass of the carriers in the QW play critical roles in the carrier transport and lead to the low efficiency of red μ-LED. Random alloy fluctuations are a natural advantage that help nitride-based LEDs to achieve higher IQE values. Similar structures to alloy fluctuations, such as quantum dot structures, could thus be introduced to red LEDs to increase their efficiency.

Author Contributions: C.-H.H. worked on simulation, data collection, and preparing the manuscript. S.-M.C. worked on data verification, modified the manuscript, and assisted with the paper's final version. Y.-R.W. supervised the simulation and code writing and revised the manuscript. All authors have read and agreed to the published version of the manuscript.

Funding: This work is supported by Ministry of Science and Technology, Taiwan (MOST) under grant Nos. 110-2923-E-002-002, 111-2923-E-002-009, and 108-2628-E-002-010-MY3).

Institutional Review Board Statement: Not applicable.

Informed Consent Statement: Not applicable.

Data Availability Statement: The datasets generated during and/or analysed during the current study are available from the corresponding author on reasonable request. The software can be downloaded at http://yrwu.ee.ntu.edu.tw, accessed on 10 February 2022.

Acknowledgments: This work is supported by MOST (Grant Nos. 110-2923-E-002-002, 111-2923-E-002-009, and 108-2628-E-002-010-MY3).

Conflicts of Interest: The authors declare no conflict of interest.

References

1. Wu, T.; Sher, C.W.; Lin, Y.; Lee, C.F.; Liang, S.; Lu, Y.; Huang Chen, S.W.; Guo, W.; Kuo, H.C.; Chen, Z. Mini-LED and micro-LED: Promising candidates for the next generation display technology. *Appl. Sci.* **2018**, *8*, 1557. [CrossRef]
2. Huang, Y.; Hsiang, E.L.; Deng, M.Y.; Wu, S.T. Mini-LED, Micro-LED and OLED displays: Present status and future perspectives. *Light. Sci. Appl.* **2020**, *9*, 105. [CrossRef] [PubMed]
3. Virey, E.H.; Baron, N. 45-1: Status and Prospects of microLED Displays. In Proceedings of the SID Symposium Digest of Technical Papers, Los Angeles, CA, USA, 20–25 May 2018; Wiley Online Library: Hoboken, NJ, USA, 2018; Volume 49, pp. 593–596.
4. Ding, K.; Avrutin, V.; Izyumskaya, N.; Özgür, Ü.; Morkoç, H. Micro-LEDs, a manufacturability perspective. *Appl. Sci.* **2019**, *9*, 1206. [CrossRef]
5. Boussadi, Y.; Rochat, N.; Barnes, J.P.; Bakir, B.B.; Ferrandis, P.; Masenelli, B.; Licitra, C. Investigation of sidewall damage induced by reactive ion etching on AlGaInP MESA for micro-LED application. *J. Lumin.* **2021**, *234*, 117937. [CrossRef]
6. Zhmakin, A.I. Enhancement of light extraction from light emitting diodes. *Phys. Rep.* **2011**, *498*, 189–241. [CrossRef]
7. Lu, S.; Li, J.; Huang, K.; Liu, G.; Zhou, Y.; Cai, D.; Zhang, R.; Kang, J. Designs of InGaN Micro-LED Structure for Improving Quantum Efficiency at Low Current Density. *Nanoscale Res. Lett.* **2021**, *16*, 99. [CrossRef]
8. Wong, M.S.; Speck, J.S.; Nakamura, S.; DenBaars, S.P. High efficiency of III-nitride and AlGaInP micro-light-emitting diodes using atomic layer deposition. In *Proceedings of the Light-Emitting Devices, Materials, and Applications XXV*; International Society for Optics and Photonics: Bellingham, WA, USA, 2021; Volume 11706, p. 117060B.
9. Zhou, S.; Cao, B.; Liu, S. Optimized ICP etching process for fabrication of oblique GaN sidewall and its application in LED. *Appl. Phys. A* **2011**, *105*, 369–377. [CrossRef]
10. Horng, R.H.; Chien, H.Y.; Chen, K.Y.; Tseng, W.Y.; Tsai, Y.T.; Tarntair, F.G. Development and fabrication of AlGaInP-based flip-chip micro-LEDs. *IEEE J. Electron Devices Soc.* **2018**, *6*, 475–479. [CrossRef]
11. Sinha, S.; Tarntair, F.G.; Ho, C.H.; Wu, Y.R.; Horng, R.H. Investigation of Electrical and Optical Properties of AlGaInP Red Vertical Micro-Light-Emitting Diodes With Cu/Invar/Cu Metal Substrates. *IEEE Trans. Electron Devices* **2021**, *68*, 2818–2822. [CrossRef]
12. Kim, T.; Leisher, P.O.; Danner, A.J.; Wirth, R.; Streubel, K.; Choquette, K.D. Photonic crystal structure effect on the enhancement in the external quantum efficiency of a red LED. *IEEE Photonics Technol. Lett.* **2006**, *18*, 1876–1878.
13. Wong, M.S.; Kearns, J.A.; Lee, C.; Smith, J.M.; Lynsky, C.; Lheureux, G.; Choi, H.; Kim, J.; Kim, C.; Nakamura, S.; et al. Improved performance of AlGaInP red micro-light-emitting diodes with sidewall treatments. *Opt. Express* **2020**, *28*, 5787–5793. [CrossRef] [PubMed]
14. Ryu, H.Y.; Shin, D.S.; Shim, J.I. Analysis of efficiency droop in nitride light-emitting diodes by the reduced effective volume of InGaN active material. *Appl. Phys. Lett.* **2012**, *100*, 131109. [CrossRef]
15. Tian, P.; McKendry, J.J.; Gu, E.; Chen, Z.; Sun, Y.; Zhang, G.; Dawson, M.D.; Liu, R. Fabrication, characterization and applications of flexible vertical InGaN micro-light emitting diode arrays. *Opt. Express* **2016**, *24*, 699–707. [CrossRef] [PubMed]
16. Akasaki, I. Key inventions in the history of nitride-based blue LED and LD. *J. Cryst. Growth* **2007**, *300*, 2–10. [CrossRef]
17. Jiang, H.; Lin, J. Nitride micro-LEDs and beyond-a decade progress review. *Opt. Express* **2013**, *21*, A475–A484. [CrossRef]
18. Wierer, J.J., Jr.; Tansu, N. III-Nitride Micro-LEDs for Efficient Emissive Displays. *Laser Photonics Rev.* **2019**, *13*, 1900141. [CrossRef]
19. Hwang, D.; Mughal, A.; Pynn, C.D.; Nakamura, S.; DenBaars, S.P. Sustained high external quantum efficiency in ultrasmall blue III–nitride micro-LEDs. *Appl. Phys. Express* **2017**, *10*, 032101. [CrossRef]
20. Shen, H.T.; Weisbuch, C.; Speck, J.S.; Wu, Y.R. Three-Dimensional Modeling of Minority-Carrier Lateral Diffusion Length Including Random Alloy Fluctuations in (In, Ga) N and (Al, Ga) N Single Quantum Wells. *Phys. Rev. Appl.* **2021**, *16*, 024054. [CrossRef]
21. der Maur, M.A.; Pecchia, A.; Di Carlo, A. Influence of random alloy fluctuations in InGaN/GaN quantum wells on LED efficiency. In Proceedings of the 2015 IEEE 1st International Forum on Research and Technologies for Society and Industry Leveraging a better tomorrow (RTSI), Turin, Italy, 16–18 September 2015; pp. 153–156.
22. Der Maur, M.A.; Pecchia, A.; Penazzi, G.; Rodrigues, W.; Di Carlo, A. Efficiency drop in green InGaN/GaN light emitting diodes: The role of random alloy fluctuations. *Phys. Rev. Lett.* **2016**, *116*, 027401. [CrossRef]
23. Yang, T.J.; Shivaraman, R.; Speck, J.S.; Wu, Y.R. The influence of random indium alloy fluctuations in indium gallium nitride quantum wells on the device behavior. *J. Appl. Phys.* **2014**, *116*, 113104. [CrossRef]
24. Ho, C.H.; Speck, J.S.; Weisbuch, C.; Wu, Y.R. Efficiency and Forward Voltage of Blue and Green Lateral LEDs with V-defects in Quantum Wells. *Phys. Rev. Appl.* **2022**, *17*, 014033. [CrossRef]
25. Li, C.K.; Wu, Y.R. Study on the current spreading effect and light extraction enhancement of vertical GaN/InGaN LEDs. *IEEE Trans. Electron Devices* **2011**, *59*, 400–407. [CrossRef]
26. Wu, Y.R.; Singh, M.; Singh, J. Sources of transconductance collapse in III-V nitrides-consequences of velocity-field relations and source/gate design. *IEEE Trans. Electron Devices* **2005**, *52*, 1048–1054. [CrossRef]
27. Chin, H.; Cheng, I.; Li, C.; Wu, Y.; Chen, J.; Lu, W.; Lee, W. Electrical properties of modulation-doped rf-sputtered polycrystalline MgZnO/ZnO heterostructures. *J. Phys. D Appl. Phys.* **2011**, *44*, 455101. [CrossRef]
28. Di Vito, A.; Pecchia, A.; Di Carlo, A.; Auf der Maur, M. Simulating random alloy effects in III-nitride light emitting diodes. *J. Appl. Phys.* **2020**, *128*, 041102. [CrossRef]
29. Chen, H.H.; Speck, J.S.; Weisbuch, C.; Wu, Y.R. Three dimensional simulation on the transport and quantum efficiency of UVC-LEDs with random alloy fluctuations. *Appl. Phys. Lett.* **2018**, *113*, 153504. [CrossRef]

30. Oh, J.T.; Lee, S.Y.; Moon, Y.T.; Moon, J.H.; Park, S.; Hong, K.Y.; Song, K.Y.; Oh, C.; Shim, J.I.; Jeong, H.H.; et al. Light output performance of red AlGaInP-based light emitting diodes with different chip geometries and structures. *Opt. Express* **2018**, *26*, 11194–11200. [CrossRef]
31. Liu, C.; Cai, Y.; Liu, Z.; Ma, J.; Lau, K.M. Metal-interconnection-free integration of InGaN/GaN light emitting diodes with AlGaN/GaN high electron mobility transistors. *Appl. Phys. Lett.* **2015**, *106*, 181110. [CrossRef]
32. Masui, H.; Nakamura, S.; DenBaars, S.P.; Mishra, U.K. Nonpolar and semipolar III-nitride light-emitting diodes: Achievements and challenges. *IEEE Trans. Electron Devices* **2009**, *57*, 88–100. [CrossRef]